Article

Photoactivatable BODIPYs Designed to Monitor the Dynamics of Supramolecular Nanocarriers

Yang Zhang, Subramani Swaminathan, Sicheng Tang, Jaume Garcia, Marcia Boulina, Burjor Captain, James D. Baker, and Françisco M. Raymo

J. Am. Chem. Soc., **Just Accepted Manuscript** • DOI: 10.1021/ja5125308 • Publication Date (Web): 20 Mar 2015

Journal of the American Chemical Society

Photoactivatable BODIPYs Designed to Monitor the Dynamics of Supramolecular Nanocarriers

Yang Zhang,† Subramani Swaminathan,† Sicheng Tang,† Jaume Garcia-Amorós,† Marcia Boulina,‡ Burjor Captain,† James D. Baker§ and Françisco M. Raymo*,†

Laboratory for Molecular Photonics, Department of Chemistry, University of Miami, 1301 Memorial Drive, Coral Gables, FL 33146-0431, Department of Biology, University of Miami, 1301 Memorial Drive, Coral Gables, FL 33146-0431 and Analytical Imaging Core Facility, Diabetes Research Institute, University of Miami, 1450 NW 10th Avenue, Miami, FL 33136

E-Mail: fraymo@miami.edu

Abstract: Self-assembling nanoparticles of amphiphilic polymers can transport hydrophobic molecules across hydrophilic media and, as a result, can be valuable delivery vehicles for a diversity of biomedical applications. Strategies to monitor their dynamics noninvasively and in real time are, therefore, essential to investigate their translocation within soft matrices and, possibly, rationalize the mechanisms responsible for their diffusion in biological media. In this context, we designed molecular guests with photoactivatable fluorescence for these supramolecular hosts and demonstrated that the activation of the fluorescent cargo, under optical control, permits the tracking of the nanocarrier translocation across hydrogel matrices with the sequential acquisition of fluorescence images. In addition, the mild illumination conditions sufficient to implement these operating principles permit fluorescence activation

† Department of Chemistry
‡ Diabetes Research Institute
§ Department of Biology

within developing *Drosophila Melanogaster* embryos and enable the monitoring of the loaded nanocarriers for long periods of time with no cytotoxic effects and no noticeable influence on embryogenesis. These photoresponsive compounds combine a borondipyrromethene (BODIPY) chromophore and a photocleavable oxazine within their covalent skeleton. Under illumination at an appropriate activation wavelength, the oxazine ring cleaves irreversibly to bring the adjacent BODIPY fragment in conjugation with an indole heterocycle. This structural transformation shifts bathochromically the BODIPY absorption and permits the selective excitation of the photochemical product with concomitant fluorescence. In fact, these operating principles allow the photoactivation of BODIPY fluorescence with large brightness and infinite contrast. Thus, our innovative structural design translates into activatable fluorophores with excellent photochemical and photophysical properties as well as provides access to a general mechanism for the real-time tracking of supramolecular nanocarriers in hydrophilic matrices.

Introduction

Amphiphilic polymers incorporate hydrophilic and hydrophobic segments within their macromolecular backbone.[1–7] In aqueous environments, multiple copies of these macromolecular constructs assemble spontaneously into single particles with nanoscaled dimensions. A subtle balance of enthalpic and entropic terms brings the hydrophobic segments of distinct polymers together in order to minimize their direct exposure to water. The concomitant solvation of the hydrophilic counterparts ensures the effective dispersion of the nanoparticles and prevents their further association into large aggregates. The overall result is the spontaneous formation of supramolecular hosts with hydrophilic surface and hydrophobic core, where molecular guests can be encapsulated. Indeed, such nanostructured constructs can capture multiple hydrophobic molecules in their interior and transport them across hydrophilic media. Furthermore, the structural design of these nanocarriers can be engineered to allow their internalization in living cells and the transfer of their cargo from the extracellular to the intracellular space. As a result, these fascinating supramolecular assemblies can become viable delivery vehicles for a diversity of biomedical applications.[8–26] In this context, the development of strategies to monitor their translocation

across soft matrices in real time, without significant perturbations of the sample, would be particularly valuable. If available, such methods would offer the opportunity to investigate and optimize the transport properties of the nanocarriers as well as facilitate the rationalization of the mechanisms responsible for their cellular internalization. Specifically, the noninvasive character of fluorescence measurements,[27] together with the ability of these supramolecular containers to preserve the photophysical properties of encapsulated chromophores,[28] would be especially convenient to design appropriate mechanisms to track the dynamics of these particular nanoparticles.

Fluorescence recovery after photobleaching (FRAP) is a valuable experimental protocol to monitor the diffusion of fluorescent species within a diversity of samples in real time.[29] It is based on the illumination of a geometrically-defined portion of the sample at the excitation wavelength (λ_{Ex}) of the chromophores with sufficiently high intensity and for an appropriately long time to bleach the emissive species and turn fluorescence off in the irradiated area. The subsequent and sequential acquisition of images, under illumination of the entire sample at λ_{Ex} with moderate intensity, then reveals the gradual recovery of fluorescence in the bleached area, if the many intact fluorophores present in the rest of the sample can slowly diffuse into this particular region. Under these conditions, the temporal dependence of the recovering emission intensity can provide quantitative information on the diffusion process. The bleaching step necessary for the local fluorescence depletion, however, limits significantly the implementation of FRAP. Indeed, the relatively high illumination intensities required for the photoinduced degradation of the emissive species can have deleterious consequences on the sample under analysis. In addition, fairly long irradiation times are often required to ensure the complete bleaching of the fluorophores, preventing the investigation of diffusion processes that occur on relatively short timescales. Furthermore, significant amounts of molecular oxygen are also necessary to ensure the photodegradation of most fluorophores, restricting the application of FRAP to oxygenated samples.

The limitations inherent to the operating principles of FRAP can be overcome with the use of photoactivatable fluorophores.[30–35] These compounds require irradiation at a given activation wavelength (λ_{Ac}), prior to illumination at λ_{Ex}, in order to produce fluorescence. Generally, the absorption

of photons at λ_{Ac} induces a photochemical reaction designed to enable the subsequent absorption at λ_{Ex} and the population of the excited state responsible for fluorescence. Alternatively, the photochemical transformation can be engineered to suppress a quenching pathway that would, otherwise, deactivate nonradiatively the excited state responsible for emission. In both instances, a concatenation of photochemical and photophysical processes ensures the activation of fluorescence exclusively after illumination at both wavelengths. Under these conditions, the irradiation of a portion of the sample, labeled with photoactivatable fluorophores, at λ_{Ac} turns fluorescence on exclusively in the illuminated area. The subsequent and sequential acquisition of images, under irradiation at λ_{Ex} of the entire specimen, then reveals the gradual decrease in emission intensity within the activated area, if the fluorescent species can slowly diffuse out of this region. Once again, the temporal evolution of the emission intensity can then provide quantitative information on the diffusion process. In contrast to the bleaching step of FRAP, however, photoactivation generally occurs efficiently even after short irradiation pulses at moderate illumination intensity and does not require any molecular oxygen. As a result of these obvious advantages, photoactivatable fluorophores are becoming invaluable tools to monitor dynamic events in a diversity of biological samples and synthetic materials.[36–41] Additionally, the spatiotemporal control of fluorescence, possible with these molecules, offers also the opportunity to overcome the limitations that diffraction imposes on the spatial resolution of conventional images and permits the visualization of structural features at the nanometer level.[42–49] In principle, the entrapment of such photoresponsive probes within the hydrophobic interior of self-assembling nanoparticles of amphiphilic polymers would enable the tracking of the resulting supramolecular constructs, and perhaps even their localization with subdiffraction resolution, on the basis of fluorescence photoactivation.

The borondipyrromethene (BODIPY) chromophore is a versatile building block for the construction of fluorescent probes.[50–55] It can be assembled conveniently from appropriate pyrrole precursors and modified in any position along the perimeter of its heterocyclic platform with established synthetic procedures. Furthermore, BODIPY derivatives generally have large molar absorption coefficients and large fluorescence quantum yields. In spite of their synthetic accessibility as well as of their excellent photophysical properties, mechanisms to photoactivate BODIPY fluorescence remain limited only to a

few representative examples.[56,57] In these systems, a photocleavable quencher is attached covalently to the BODIPY platform in order to suppress fluorescence. Specifically, excitation of the BODIPY chromophore at λ_{Ex} results in the transfer of one electron to or from the quencher, instead of the radiative deactivation of the former. Illumination at λ_{Ac}, however, cleaves the covalent linkage between quencher and fluorophore. The physical separation of the two prevents electron transfer upon excitation of the latter and ensures fluorescence instead. Nonetheless, these photoactivation mechanisms translate into minimal changes in the absorption spectrum of the BODIPY chromophore. As a result, absorption at λ_{Ex} occurs before and after activation and, unless the quenching mechanism is designed to be extremely efficient, noticeable background fluorescence is detected. Additionally, the lack of any significant change in absorption with activation prevents the possibility to bleach selectively the activated state and, hence, to implement schemes for subdiffraction imaging.[58–64] Indeed, the exclusive bleaching of the emissive species, after their localization at the single-molecule level, is an essential step in the sequential reconstruction of images with subdiffraction resolution on the basis of fluorescence activation. Thus, the identification of alternative operating principles to activate the emission of BODIPY chromophores with concomitant changes in absorption would be particularly valuable to develop photoactivatable fluorophores with optimal photochemical and photophysical properties to monitor diffusion as well as to acquire superresolution images. In particular, the attachment of a BODIPY chromophore to a photoswitchable auxochrome, instead of a photocleavable quencher, appears to be a viable strategy to regulate the absorption characteristics of the emissive component under optical control. Such structural design should provide the opportunity to photoinduce a sufficient shift in the BODIPY absorption to permit the selective excitation of the photochemical product in the presence of the corresponding reactant. As a result, infinite fluorescence contrast and exclusive product bleaching can in principle be achieved on the basis of this mechanism for the photoactivation of BODIPY emission.

In search of strategies to photoactivate fluorescence, we developed a family of molecular dyads integrating fluorescent and photochromic components within the same covalent skeleton.[65] Upon illumination at λ_{Ac}, the heterocyclic core of the photochrome opens to extend the electronic conjugation of the fluorophore. This structural transformation shifts bathochromically the main absorption band of

the fluorophore and permits the exclusive excitation of the photogenerated state at λ_{Ex}. The photochemical reaction responsible for fluorescence activation, however, is thermally reversible. The fluorescent state survives only for a few microseconds before reverting to the initial species. As a result, dynamic processes occurring on timescales that are longer than the lifetime of the activated species cannot be monitored with these photoswitchable systems. In order to overcome this limitation, we envisaged the possibility of modifying the structural design of the photochromic component of our dyads to enable the irreversible, rather than reversible, activation of their fluorescence. In this article, we report the implementation of these operating principles as well as demonstrate that they can be employed to activate irreversibly the fluorescence of BODIPY chromophores and monitor the translocation of supramolecular nanocarriers in soft matrices.

Results and Discussion

Design, Synthesis and Structural Characterization: The photochromic component of our switchable molecular dyads fuses 2*H*,3*H*-indole and 2*H*,4*H*-benzo[1,3]oxazine heterocycles within its molecular skeleton (***a*** in Figure 1).[66] The latter fragment incorporates a nitro group in the *para*-position, relative to the oxygen atom, and is responsible for absorbing the activating photons at λ_{Ac}. Upon excitation, the [C–O] bond at the junction of the two heterocyclic fragments cleaves to open the oxazine ring and generate a zwitterionic isomer (***b*** in Figure 1). The photogenerated species then reverts back spontaneously to the original state with first-order kinetics. In addition to the cleaving [C–O] bond, also a [C–N] bond between the nitrogen atom and the adjacent benzyl group holds the oxazine ring together. The relocation of the nitro group from the *meta*- to the *ortho*-position, relative to the benzyl group, is expected to allow the irreversible photochemical opening of the oxazine heterocycle. Indeed, *ortho*-nitrobenzyl derivatives are common photocleavable protecting groups that convert irreversibly into the corresponding *ortho*-nitrosobenzaldehydes.[67] On the basis of these considerations, we designed compound **1** and its BODIPY conjugates **2** and **3** (Figure 2). The [C–N] bond of their *ortho*-nitrobenzyl group is expected to cleave, upon illumination at an appropriate λ_{Ac}, and generate corresponding 3*H*-indoles **4**–**6**, after the elimination of *ortho*-nitrosobenzaldehyde **7**.

Compound **1** was synthesized in three steps from 2-methyl-3-methoxynitrobenzene (Figure 3). Specifically, bromination of the methyl group to generate **8**, cleavage of the methoxy group to produce **9** and condensation with **4** afford the target oxazine in an overall yield of 8%. The structural identities of the intermediates and final compound were confirmed by electrospray ionization mass spectrometry (ESIMS), ^{1}H and ^{13}C nuclear magnetic resonance (NMR) spectroscopies. In addition, single crystals of **1**, suitable for X-ray diffraction analysis (Table S1), could be obtained from an acetonitrile solution of the compound. The resulting structure (Figure 4) clearly reveals the oxazine core of this molecule together with the nitro substituent in the *ortho*-position, relative to the benzyl group, necessary to induce the designed photochemical transformation.

The covalent attachment of BODIPY chromophores to the methyl group on the chiral center of **1** can be performed in a single additional synthetic step (Figure 3). In particular, condensation of **1** with **10** or **11** generates **2** or **3** in yields of 15 or 17% respectively. Once again, the structural identities of the resulting BODIPY–oxazine dyads were confirmed by ESIMS as well as ^{1}H and ^{13}C NMR spectroscopies. In addition, the ^{1}H NMR spectra of both compounds reveal an AX system for the pair of protons on the ethyne bridge, separating the two functional components of each dyad, with coupling constants of 16 and 17 Hz respectively. These relatively large values demonstrate that the associated [C=C] bond adopts a *trans* configuration in both compounds.

Photochemical and Photophysical Properties: Illumination of an acetonitrile solution of **1** at a λ_{Ac} of 350 nm results in the cleavage of the *ortho*-nitrobenzyl group with the formation of **4** and **7** (Figure 2), in agreement with the logic behind the design of this particular oxazine. The progress of the photochemical transformation can be monitored conveniently by high-performance liquid chromatography (HPLC) and absorption spectroscopy. In particular, chromatograms (Figure 5), recorded at regular intervals of time during photolysis, reveal the gradual decrease of a peak with a retention time of 13 min and the concomitant growth of a peak with a retention time of 4 min. These peaks correspond to **1** and **4** respectively and the temporal dependence of their intensities indicates the activation quantum yield for the transformation of the reactant into the product to be 0.043 (ϕ_A in Table

1). Similarly, spectra (Figure 6), recorded during photolysis, show a decrease in absorbance for the bands of **1** at 236 and 277 nm together with the concomitant growth of the characteristic absorption of an *ortho*-nitrosobenzaldehyde chromophore at *ca.* 400 nm, consistently with the photoinduced formation of **7**.

The absorption spectrum (***a*** in Figure 7) of model compound **12** shows a band at 521 nm (λ_{Ab} in Table 1) for its BODIPY chromophore. Covalent attachment of this chromophoric unit to the photocleavable oxazine has a negligible influence on its absorption in the case of **2** (***b*** in Figure 7), while it shifts the band to 548 nm for **3** (***d*** in Figure 7). Presumably, steric hindrance prevents the ethyne bridge from adopting a co-planar arrangement with the adjacent chromophoric fragment in the ground state of **2**. Its geometry, however, appears to relax significantly in the excited state and, in fact, the Stokes shift of **2** is 25 nm, while those of **12** and **3** are only 13 and 14 nm respectively. Specifically, the BODIPY emission appears at 534, 555 and 562 nm for **12**, **2** and **3** respectively (λ_{Em} in Table 1 and Figure S1). Nonetheless, the fluorescence quantum yields of **2** and **3** are only 0.06 and 0.07 respectively (ϕ_F in Table 1), while that of **12** is 0.77. Thus, the proximal oxazine component tends to encourage the nonradiative deactivation of the BODIPY fluorophore in both dyads. Presumably, electron transfer either from the nitrogen atom of the 2*H*,3*H*-indole heterocycle to the excited BODIPY or from the excited chromophore to the nitro group on the adjacent phenoxy fragment is responsible for this behavior. Indeed, the redox potentials of **1** and **12** suggest that both electron-transfer processes are exergonic with free-energy changes of –0.18 and –0.30 eV respectively.[68]

In analogy to the photochemical behavior of **1**, illumination of **2** and **3** at a λ_{Ac} of 350 nm cleaves their *ortho*-nitrobenzyl group to generate **5** and **6** respectively together with **7**. Consistently, the absorption spectra (***a*** and ***b*** in Figure 8) of acetonitrile solutions of the two dyads reveal a decrease in the absorbance of their BODIPY fragments at 520 and 548 nm respectively during photolysis. Furthermore, a band for the *ortho*-nitrosobenzaldehyde chromophore of **7** develops between 300 and 400 nm in both instances and an absorption for the BODIPY fragments of **5** and **6** appears at 534 and 588 nm respectively. In fact, the latter absorptions are identical to those observed for the isolated compounds (***c*** and ***e*** in Figure 7). Thus, the photoinduced transformation of **2** into **5** and of **3** into **6** shifts bathochromically the BODIPY

absorption by 14 and 40 nm respectively. Such a shift offers the opportunity to excite exclusively the BODIPY chromophore of the photochemical product by illuminating the sample at a λ_{Ex} positioned within the developing absorption. Nonetheless, excitation of **5** produces only a weak emission at 620 nm with a fluorescence quantum yield lower than 0.01 (Table 1 and Figure S1). By contrast, **6** emits at 602 nm with a fluorescence quantum yield of 0.50. This particular value in conjunction with a molar absorption coefficient of 134 mM^{-1} cm^{-1} (ε in Table 1) at λ_{Ab} corresponds to a brightness of 67 mM^{-1} cm^{-1} ($\varepsilon \times \phi_F$ in Table 1). Such a combination of photophysical properties translates into the activation of intense fluorescence with the photochemical conversion of **3** into **6**. In fact, emission spectra (***c*** in Figure 8), recorded with a λ_{Ex} of 580 nm at regular intervals of time during photolysis at a λ_{Ac} of 350 nm, show the appearance and growth of the characteristic band of the photochemical product. Therefore, this particular choice of chromophoric building blocks offers the opportunity to activate the emission of a bright fluorophore on the basis of the interplay between activating and exciting sources in conjunction with a mechanism that enables the selective excitation of the product, satisfying all the requirements behind the rationale for the design of these molecular switches.

The chromophoric fragments of **3** are relatively hydrophobic and, as a result, this dyad is essentially insoluble in aqueous solutions. However, it dissolves readily in phosphate buffer saline (PBS, pH = 7.4) under the assistance of **13** (Figure 9). This particular macromolecular construct has a number average molecular weight (M_n) of 30 kDa and incorporates hydrophilic oligo(ethylene glycol) and hydrophobic decyl side chains in a ratio of 3:1 along a common poly(methacrylate) backbone.[69] In aqueous environment at concentrations greater than 5.7 μg mL^{-1}, multiple copies of this polymer assemble spontaneously into particles with an average hydrodynamic diameter of 31 nm.[70] The resulting supramolecular hosts can capture molecular guests in their hydrophobic interior.[65d,f,g,j,71] Indeed, the absorption spectrum of nanoparticles of **13**, loaded with **3**, reveals the characteristic BODIPY absorption at 550 nm (***a*** in Figure 9). Upon illumination at a λ_{Ac} of 350 nm, **3** switches to **6** within the interior of the nanoparticles and the characteristic absorption band of the product appears at 596 nm (***b*** in Figure 9). Irradiation at a λ_{Ex} positioned within this band excites **6** selectively with the concomitant appearance of an emission at 607 nm in the corresponding spectrum (***c*** in Figure 9). Thus, the switchable dyad retains

its photochemical and photophysical properties essentially unaltered, despite encapsulation within the supramolecular containers.

Fluorescence Imaging: The emission bands (***c*** and ***d*** in Figure S1) of **3** and **6** are sufficiently resolved to permit the monitoring of the photochemical conversion of one compound into the other with two independent detection channels. Specifically, illumination of a rectangular portion of a poly(butyl methacrylate) (PBMA) film, doped with the dyad, at a λ_{Ac} of 405 nm converts **3** into **6** exclusively within the irradiated area. The subsequent acquisition of an image (***a*** in Figure 10) with a λ_{Ex} of 514 nm, where **3** absorbs, and a detection window of 530–650 nm, where **3** emits, shows significant fluorescence only outside the activated area. By contrast, an image (***b*** in Figure 10) of the very same sample collected with a λ_{Ex} of 594 nm, where **6** absorbs, and a detection window of 610–700 nm, where **6** emits, shows significant fluorescence exclusively within the activated area. Furthermore, exactly the same fluorescent square can be observed in images (Figure S4) collected with these excitation and detection conditions several minutes after activation. These results confirm the photoinduced conversion of **3** into **6** and demonstrate that the photochemical product cannot diffuse within the rigid polymer matrix.

The fluorescence activation associated with the transformation of **3** into **6** can be exploited to monitor the translocation of nanoparticles of **13** across soft matrices. In particular, these supramolecular nanocarriers can be loaded with **3** and dispersed in an alginate hydrogel.[72–75] An image of the resulting sample (***a*** in Figure 11), recorded with a λ_{Ex} of 594 nm and a detection window of 610–700 nm, does not reveal any significant fluorescence. Illumination of a rectangular area at the center of the imaging field at λ_{Ac} of 405 nm converts **3** into **6** and causes the appearance of intense emission in this particular portion of the sample (***b*** in Figure 11). The nanocarriers with activated cargo, however, can gradually diffuse across the soft hydrogel matrix.[76] As a result, an image (***c*** in Figure 11), recorded 630 s after activation, clearly reveals fluorescence outside the activated area because of the translocation of the emissive species across the sample. In fact, the sequential acquisition of images after activation offers the opportunity to monitor this dynamic process in real time (Video S1). The very same process can also be tracked with conventional FRAP schemes (Figure S5 and Video S2) and nanoparticles of **13** containing **12**. However,

the illumination time required to bleach **12** is significantly longer than that sufficient to activate **3**, under otherwise identical conditions. Specifically, illumination at 405 nm for only 10 s converts a sufficient amount of **3** into **6** to permit the detection of fluorescence against a dark background, while it has negligible influence on the images recorded with **12** (***a*** and ***b*** in Figure S5). The latter compound requires an illumination time of, at least, 60 s to enable the effective suppression of fluorescence and the subsequent tracking of the nanoparticle diffusion (***a***–***c*** in Figure S5).

The relatively mild illumination conditions sufficient to convert **3** into **6**, in conjunction with the photophysical properties of both compounds, are particularly attractive to probe dynamics within living organisms. In particular, the fate of nanoparticles of **13**, containing **3** and microinjected within a *Drosophila Melanogaster* embryo during cellularization,[77] can be monitored conveniently on the basis of the photoactivation of their fluorescent cargo. Overlaid fluorescence and transmittance images (***a*** in Figure 12) of a labeled embryo, positioned next to an unlabeled counterpart, clearly reveal the intense emission of the fluorescent nanocarriers exclusively in the former. In this particular experiment, the imaging field was illuminated at a λ_{Ex} of 514 nm, where **3** absorbs, and fluorescence was detected within 530–650 nm, where **3** emits. Irradiation of a relatively small region (arrow in ***b*** of Figure 12) within the labeled embryo at 405 nm converts **3** into **6** and causes a pronounced decrease in emission, detected under the same conditions, exclusively in the activated area. Instead, the corresponding images (***c*** and ***d*** in Figure 12) recorded with a λ_{Ex} of 594 nm, where **6** absorbs, and a detection window of 610–700 nm, where **6** emits, show the appearance of intense fluorescence in the activated area of the labeled embryo, in agreement with the photoinduced generation of this particular compound. Furthermore, the subsequent acquisition of frames over the course of 2250 s does not reveal any spatial redistribution of the activated nanoparticles (Video S3). The final image (Figure S7), acquired after this relatively long period of time, is essentially identical to that recorded immediately after activation (***d*** in Figure 12). These observations demonstrate that the fluorescent nanocarriers cannot diffuse within the developing embryos, in contrast to their ability to translocate within the microporous alginate hydrogel (***a***–***c*** in Figure 11 and Video S1). Presumably, the nanoparticles remain immobilized within the many hydrophobic domains present in the growing embryo.[77] Additionally, comparison of the labeled and unlabeled embryos over this period of

time does not show any significant difference in their development (Video S3). Both undergo gastrulation and continue to grow even after photoactivation, indicating that the illumination conditions and photochemical products do not have any noticeable cytotoxic effects and influence on the subsequent steps of embryogenesis.

Conclusions

A photocleavable 2*H*,4*H*-benzo[1,3]oxazine can be assembled in three synthetic steps from a commercial precursor and condensed to formylated BODIPYs in a further synthetic step. Illumination of the resulting BODIPY–oxazine dyads at an appropriate λ_{Ac} cleaves the oxazine ring irreversibly and brings the corresponding BODIPY chromophore in conjugation with a 3*H*-indole heterocycle. This structural transformation shifts bathochromically the BODIPY absorption by up to 40 nm and allows the selective excitation of the photochemical product at an appropriate λ_{Ex} with concomitant emission. The molar absorption coefficients of the photogenerated species are in excess of 10^5 M^{-1} cm^{-1} with fluorescence quantum yields approaching 0.5. Furthermore, the hydrophobic character of these photoresponsive molecules encourages their encapsulation within the interior of self-assembling nanoparticles of amphiphilic polymers. In aqueous environments, the resulting supramolecular hosts retain their molecular guests and preserve their photochemical and photophysical properties. Indeed, the fluorescence of the entrapped BODIPY–oxazine dyads can be, once again, activated irreversibly under the influence of illuminating sources operating at λ_{Ac} and λ_{Ex}. In turn, the translocation of supramolecular nanocarriers with activated cargo across an alginate hydrogel matrix can be probed in real time with the sequential acquisition of fluorescence images. Additionally, the illumination conditions required to activate the fluorescence of these photoresponsive probes are significantly milder than those needed to bleach a conventional fluorophore and implement a FRAP scheme. In fact, the fluorescent cargo of nanocarriers, microinjected within developing *Drosophila Melanogaster* embryos, can be photoactivated and then monitored for prolonged periods of time without cytotoxic effects and any noticeable influence on embryogenesis. Thus, this particular structural design to photoactivate BODIPY fluorescence with

large brightness and infinite contrast can evolve into a general experimental protocol to track the dynamics of supramolecular nanocarriers and their cargo across soft matrices in real time.

Experimental Section

Materials and Methods: Chemicals were purchased from commercial sources and used as received. CH_2Cl_2 and MeCN were distilled over CaH_2. THF was distilled over Na and benzophenone. H_2O (18.2 MΩ cm) was purified with a Barnstead International NANOpure DIamond Analytical system. Decyl methacrylate, poly(ethylene glycol) methyl ether methacrylate, 1,4-bis(2-bromo-2-methylpropionato)benzene, **10** and **12** were prepared according to literature procedures.[56,65e,71a,78] ESIMS was performed with a Bruker micrOTO-Q II spectrometer. NMR spectra were recorded with a Bruker Avance 400 spectrometer. HPLC traces were acquired with a Varian ProStar system, equipped with a ProStar 330 photodiode array detector (250 nm), using an Agilent Microsorb 100-5 BDS column (4.6 × 250 mm) and a MeCN/H_2O (60:40, v/v) eluent (1.0 mL min^{-1}). GPC analyses were performed with the same chromatographic apparatus, using a Phenogel 5-μm 10E4A column (7.8 × 300 mm) and a THF eluent (1.0 mL min^{-1}). Monodisperse polystyrene standards (2,700–200,000) were employed to determine the M_n and PDI of the polymers from the GPC traces. DLS measurements were performed with a Malvern ZEN1600 apparatus. Absorption spectra were recorded with a Varian Cary 100 Bio spectrometer in quartz cells with a path length of 1.0 cm. Emission spectra were recorded with a Varian Cary Eclipse spectrometer in aerated solutions. The values of ϕ_F were determined against cresyl violet and rhodamine 6G standards, following a literature protocol.[27] Those of ϕ_A were determined with a potassium ferrioxalate actinometer, according to an established procedure.[79] Solutions were irradiated at 350 nm (4.88 mW cm^{-2}) with a Luzchem Research LZC-4V photoreactor. Voltammograms were recorded with a CH Instruments 610A electrochemical analyzer in MeCN under Ar, using a three-electrode cell. The reference was a Ag/Ag^+ electrode (1 mM $AgNO_3$ in MeCN). The counter and working were a platinum wire and a glassy-carbon electrode respectively. The supporting electrolyte was Bu_4NPF_6 (0.1 M). The scan rate and pulse amplitude were 50 mV s^{-1} and 50 mV respectively. Fluorescence images were recorded with a Leica SP5 confocal laser-scanning microscope.

1. A solution of **4** (549 mg, 3.4 mmol) and **9** (800 mg, 3.4 mmol) in MeCN (10 mL) was heated for 12 hours under reflux and Ar. After cooling down to ambient temperature, the solvent was distilled off under reduced pressure. The residue was dissolved in CH_2Cl_2 (50 mL) and washed with H_2O (20 mL). The organic layer was dried over Na_2SO_4 and the solvent was distilled off under reduced pressure. The residue was purified by column chromatography [SiO_2, hexanes/AcOEt (95:5, v/v)] to give **1** (150 mg**,** 14%) as a yellow solid. ESIMS: *m/z* = 311.1401 $[M + H]^+$ (*m/z* calcd. for $C_{18}H_{19}N_2O_3$ = 311.1390); ^1H NMR (CD_3CN): δ = 1.17 (3H, s), 1.53 (3H, s), 1.60 (3H, s), 4.86 (1H, d, 16 Hz), 5.04 (1H, d, 16 Hz), 6.66 (1H, d, 8 Hz), 6.79–6.83 (1H, m), 6.98–7.05 (2H, m), 7.17 (1H, d, 8 Hz), 7.28 (1H, t, 8 Hz), 7.67 (1H, d, 8 Hz); ^{13}C NMR ($CDCl_3$): δ = 16.1, 18.8, 25.8, 38.9, 47.8, 100.6, 108.3, 116.0, 117.1, 120.3, 122.4, 123.9, 127.6, 137.9, 146.8, 147.7, 154.7.

2. A solution of **1** (100 mg, 0.3 mmol), **10** (113 mg, 0.3 mmol) and trifluoroacetic acid (TFA, 0.1 mL, 1.3 mmol) in EtOH (10 mL) was heated for 24 hours under reflux. After cooling down to ambient temperature, the solvent was distilled off under reduced pressure and the residue was dissolved in CH_2Cl_2 (5 mL). The addition of hexane (50 mL) caused the precipitation of a solid, which was filtered off, dissolved in CH_2Cl_2 (20 mL) and washed with H_2O (20 mL). The organic phase was dried over Na_2SO_4 and the solvent was distilled off under reduced pressure. The residue was purified by column chromatography [SiO_2, hexanes/EtOAc (90:10, v/v)] to give **2** (30 mg, 15%) as a red solid. ESIMS: *m/z* = 645.2837 $[M + H]^+$ (*m/z* calcd. for $C_{38}H_{36}BF_2N_4O_3$ = 645.2849); ^1H NMR (CD_3CN): δ = 1.18 (3H, s), 1.29 (3H, s), 1.38 (3H, s), 1.51 (3H, s), 2.50 (6H, s), 4.77 (1H, d, 18 Hz), 5.01 (1H, d, 18 Hz), 5.98 (1H, d, 16 Hz), 6.14 (1H, s), 6.65 (1H, 16 Hz), 6.71 (1H, d, 8 Hz), 6.83 (1H, t, 7 Hz), 7.07 (1H, t, 7 Hz), 7.11–7.22 (2H, m), 7.28 (1H, t, 8 Hz), 7.35 (2H, bs), 7.43–7.61 (3H, m), 7.65 (1H, d, 8Hz); ^{13}C NMR ($CDCl_3$): δ = 157.0, 155.0, 153.4, 147.4, 146.8, 144.2, 142.0, 138.5, 138.0, 134.9, 129.3, 129.2, 129.1, 128.0, 127.6, 127.5, 127.2, 125.5, 123.4, 122.3, 120.4, 117.3, 117.1, 108.7, 101.9, 49.5, 39.7, 34.7, 31.6, 26.5, 25.3, 22.7, 18.3, 14.7, 14.5, 14.1, 13.7, 12.8.

3. A solution of **1** (97 mg, 0.3 mmol), **11** (100 mg, 0.3 mmol) and TFA (0.1 mL, 1.3 mmol) in EtOH (10 mL) was heated for 24 hours under reflux. After cooling down to ambient temperature, the solvent was

distilled off under reduced pressure. The residue was dissolved in CH_2Cl_2 (30 mL) and washed with a saturated aqueous solution of $NaHCO_3$ (2 × 20 mL). The organic layer was dried over Na_2SO_4 and the solvent was distilled off under reduced pressure. The residue was purified by column chromatography [SiO_2, hexanes/AcOEt (95:5 → 90:10, v/v) to give **3** (30 mg, 17%) as a dark violet solid. ESIMS: *m/z* = 687.3338 $[M + H]^+$ (*m/z* calcd. for $C_{41}H_{42}BF_2N_4O_3$ = 687.3318); ^{1}H NMR (CD_3CN): δ = 0.97 (6H, q, 8 Hz), 1.24 (3H, s), 1.28 (3H, s), 1.31 (3H, s), 1.59 (3H, s), 2.35 (2H, q, 8 Hz), 2.43–2.52 (5H, m), 4.88 (1H, d, 19 Hz), 5.08 (1H, d, 19 Hz), 6.50 (1H, d, 17 Hz), 6.77 (1H, d, 8 Hz), 6.87 (1H, td, 1 and 8 Hz), 7.10 (1H, td, 1 and 8 Hz), 7.15–7.26 (2H, m), 7.26–7.32 (1H, m), 7.31–7.34 (3H, m), 7.51–7.57 (3H, m), 7.69 (1H, dd, 1 and 8 Hz); ^{13}C NMR (CD_3CN): δ = 158.3, 154.6, 147.7, 147.0, 145.2, 141.4, 140.9, 138.1, 137.9, 135.1, 135.0, 132.7, 132.5, 131.0, 129.8, 129.2, 129.1, 128.2, 127.9, 127.6, 126.9, 123.4, 123.2, 122.4, 122.3, 120.5, 118.0, 109.0, 102.1, 49.8, 39.5, 29.4, 25.6, 17.7, 17.5, 16.5, 13.6, 12.2, 11.2, 10.6.

5. A solution of **4** (159 mg, 1.0 mmol), **10** (352 mg, 1.0 mmol) and TFA (0.1 mL, 1.3 mmol) in EtOH (20 mL) was heated for 24 hours under reflux. After cooling down to ambient temperature, the solvent was distilled off under reduced pressure and the residue was dissolved in CH_2Cl_2 (5 mL). The addition of hexane (50 mL) caused the precipitation of a solid, which was filtered off, dissolved in CH_2Cl_2 (20 mL) and washed with H_2O (20 mL). The organic phase was dried over Na_2SO_4 and the solvent was distilled off under reduced pressure. The residue was purified by column chromatography [SiO_2, hexanes/EtOAc (90:10, v/v)] to give **5** (104 mg, 21%) as a black solid. ESIMS: *m/z* = 494.2601 $[M + H]^+$ (calcd. for $C_{31}H_{31}BF_2N_3$ = 494.2579); ^{1}H NMR (CD_3CN) δ = 1.39 (6H, s), 1.42 (3H, s), 1.55 (3H, s), 2.55 (3H, s), 2.73 (3H, s), 6.20 (1H, s), 6.68 (1H, d, 17 Hz), 7.23 (1H, t, 11 Hz), 7.32 (1H, t, 8 Hz), 7.36–7.46 (3H, m), 7.51 (1H, d, 8 Hz), 7.56–7.62 (3H, m), 7.64 (1H, d, 17 Hz); ^{13}C NMR ($CDCl_3$): δ = 183.7, 157.7, 154.6, 154.0, 146.3, 144.8, 142.1, 139.5, 134.9, 132.4, 130.9, 129.4, 129.3, 129.2, 128.0, 127.8, 125.3, 122.3, 121.1, 120.5, 120.4, 52.5, 31.6, 24.0, 22.7, 14.8, 14.6, 14.2, 14.1, 13.0.

6. A solution of **4** (50 mg, 0.3 mmol), **11** (100 mg, 0.3 mmol) and TFA (0.1 mL, 1.3 mmol) in MeCN (20 mL) was heated for 24 hours under reflux. After cooling down to ambient temperature, the solvent was distilled off under reduced pressure. The residue was dissolved in CH_2Cl_2 (20 mL) and washed with

a saturated aqueous solution of $NaHCO_3$ (2 × 20 mL). The organic layer was dried over Na_2SO_4 and the solvent was distilled off under reduced pressure. The residue was purified by column chromatography [SiO_2, hexanes/AcOEt (80:20 → 30:70, v/v) to give **6** (50 mg, 36%) as a dark purple solid. ESIMS: *m/z* = 536.3050 $[M + H]^+$ (*m/z* calcd. for $C_{34}H_{37}BF_2N_3$ = 536.3049); ^1H NMR (CD_3CN): δ = 1.04 (3H, t, 8 Hz), 1.16 (3H, 8 Hz), 1.31 (3H, s), 1.37 (3H, s), 1.78 (6H, s) 2.37 (2H, q, 8 Hz), 2.58–2.80 (5H, m), 7.29–7.36 (2H, m), 7.36–7.48 (3H, m), 7.51–7.62 (4H, m), 7.85 (1H, d, 6 Hz), 8.50 (1H, d, 17 Hz); ^{13}C NMR ($CDCl_3$): δ = 183.8, 182.7, 162.2, 152.2, 144.4, 143.1, 140.4, 139.9, 137.3, 136.4, 134.7, 129.5, 129.5, 129.0, 128.0, 127.9, 124.9, 121.7, 119.4, 118.0, 100.0, 52.1, 25.3, 18.4, 17.2, 14.1, 13.9, 12.2, 10.9.

8. A solution of 2-methyl-3-methoxynitrobenzene (1.0 g, 6.0 mmol), azobis(*i*-butyronitrile) (AIBN, 98 mg, 0.1 mmol) and *N*-bromosuccinimide (NBS, 1.3 g, 7.3 mmol) in CCl_4 (15 mL) was heated for 14 hours under reflux and Ar. After cooling down to ambient temperature, the reaction mixture was diluted with CH_2Cl_2 (30 mL) and was washed with H_2O (20 mL). The organic layer was dried over Na_2SO_4 and the solvent was distilled off under reduced pressure to give **8** (1.2 g, 82%) as a white solid. ESIMS: *m/z* = 245.9760 $[M + H]^+$ (*m/z* calcd. for $C_8H_9BrNO_3$ = 245.9760); ^1H NMR ($CDCl_3$): δ = 4.00 (3H, s), 4.84 (2H, s), 7.18 (1H, bs), 7.45 (1H, d, 8Hz), 7.55 (1H, d, 8 Hz); ^{13}C NMR ($CDCl_3$): δ = 22.0, 57.4, 115.6, 117.1, 121.6, 130.0, 149.8, 158.5.

9. A solution of BBr_3 in CH_2Cl_2 (1 M, 12.7 mL) was added dropwise to a solution of **8** (1.2 g, 4.9 mmol) in CH_2Cl_2 (10 mL) maintained at –78 °C under inert atmosphere. The reaction mixture was allowed to warm up to ambient temperature, stirred for a further 12 hours, poured into H_2O (10 mL) and extracted with CH_2Cl_2 (30 mL). The organic layer was dried over Na_2SO_4 and the solvent was distilled off under reduced pressure. The residue was dissolved in AcOEt (10 mL) and filtered through a silica plug, which was washed thoroughly with AcOEt. The solvent was distilled off under reduced pressure to give **9** (800 mg, 71%) as a brown solid. ESIMS: *m/z* = 231.9604 $[M + H]^+$ (*m/z* calcd. for $C_7H_7BrNO_3$ = 231.9604); ^1H NMR (CD_3CN): δ = 4.78 (2H, s), 7.23 (1H, d, 8 Hz), 7.39 (1H, t, 8 Hz), 7.49 (1H, d, 8 Hz); ^{13}C NMR (CD_3OD): δ 21.7, 115.6, 119.3, 120.0, 129.7, 150.1, 157.2.

11. A degassed solution of 2,3-dichloro-5,6-dicyano-1,4-benzoquinone (DDQ, 474 mg, 2.1 mmol) in tetrahydrofuran (10 mL) was added dropwise to a solution of **12** (200 mg, 0.5 mmol) in tetrahydrofuran (15 mL) and H_2O (0.15 mL) maintained at 0 °C under Ar. The mixture was allowed to warm up to ambient temperature, stirred for a further 12 hours under these conditions, diluted with AcOEt (30 mL) and washed with H_2O (2 × 20 mL). The organic layer was dried over Na_2SO_4 and the solvent was distilled off under reduced pressure. The residue was purified by column chromatography [SiO_2, hexanes/AcOEt (95:5 → 80:20, v/v) to give **11** (96 mg, 47%) as a brown solid. ESIMS: *m/z* = 417.1920 $[M + Na]^+$ (*m/z* calcd. for $C_{23}H_{25}BF_2N_2ONa$ = 417.1926); ^{1}H NMR ($CDCl_3$,): δ = 1.03 (6H, t, 8 Hz), 1.28 (3H, s), 1.37 (3H, s), 2.36 (2H, q, 8 Hz), 2.65 (3H, s), 2.70 (2H, q, 8 Hz), 7.30 (2H, m), 7.54 (3H, m), 10.41 (1H, s); ^{13}C NMR ($CDCl_3$): δ = 10.5, 12.3, 13.7, 14.1, 14.4, 17.1, 17.6, 127.8, 129.5, 129.5, 132.2, 134.52, 134.6, 135.7, 137.7, 139.8, 142.1, 143.9, 166.1, 186.

13. A mixture of decyl methacrylate (1.70 g, 75 mmol), poly(ethylene glycol) methyl ether methacrylate (5.17 g, 2.5 mmol), 1,4-bis(2-bromo-2-methylpropionato)benzene (8 mg, 0.02 mmol), $FeCl_3 \cdot 6H_2O$ (3 mg, 0.01 mmol), Ph_3P (3 mg, 0.01 mmol), AIBN (8.2 mg, 0.05 mmol) in degassed THF (30 mL) was heated at 75 °C for 48 hours in a sealed tube. After cooling down to ambient temperature, the solvent was distilled off under reduced pressure and the residue was purified by column chromatography [SiO_2, CH_3Cl/MeOH (95:5, v/v)] to give **13** (513 mg, 8%) as a white solid. GPC: M_n = 30 kDa, PDI = 1.56; ^{1}H NMR ($CDCl_3$,): δ = 0.81–1.16 (25H, m), 1.20–1.45 (48H, m), 3.38 (3H, s), 3.54–3.78 (146H, m), 3.86–4.01 (6H, m), 4.04–4.20 (2H, m).

Crystallographic Analysis. Single crystals of **1** were obtained after maintaining an acetonitrile solution of the compound at ambient temperature in a sealed tube. The data crystal was glued onto the end of a thin glass fiber. X-Ray intensity data were measured with a Bruker SMART APEX2 CCD-based diffractometer, using Mo Kα radiation (λ = 0.71073 Å).[80] The raw data frames were integrated with the SAINT+ program by using a narrow-frame integration algorithm. Corrections for Lorentz and polarization effects were also applied with SAINT+. An empirical absorption correction based on the multiple measurement of equivalent reflections was applied using the program SADABS. The structure

was solved by a combination of direct methods and difference Fourier syntheses and refined by full-matrix least-squares on F^2 with the SHELXTL software package.[81] Hydrogen atoms were placed in geometrically idealized positions and included as standard riding atoms during the least-squares refinements. Crystal data, data collection parameters and results of the analyses are listed in Table S1. Compound **1** crystallized in the monoclinic crystal system. The systematic absences in the intensity data identified the unique space group $P2_1/n$.

Polymer Nanoparticles. Doped polymer nanoparticles were prepared by combining $CHCl_3$ solutions of **3** (0.1 mg mL^{-1}, 50 μL) and **13** (2.5 mg mL^{-1}, 200 μL) and heating the resulting mixture at 40 °C in an open vial. After the evaporation of the solvent, the residue was purged with air, dispersed in PBS (1 mL, pH =7.4), sonicated for 5 min and flashed through a syringe filter with a pore size of 0.2 μm. The filtrate was used for the imaging and spectroscopic measurements without further purification.

Polymer Films. Doped polymer films were prepared by spin coating CH_2Cl_2 solutions of PBMA (M_W = 337 × 10^3, 20 mg mL^{-1}) and **3** (50 μg mL^{-1}) with a Chemat Technologies KW-4A spin coater at 1200 rpm for 60 s on glass coverslips.

Alginate Hydrogels. Doped alginate hydrogels were prepared by mixing a solution of sodium alginate (20 mg mL^{-1}) in H_2O (200 μL) with a solution of nanoparticles of **13** (500 μg mL^{-1}), loaded with either **3** or **12** (5 μg mL^{-1}), in H_2O (200 μL) and then adding a drop of the mixture to a solution of $CaCl_2$ (0.24 M) in H_2O (1 mL). The resulting doped alginate bead was rinsed with H_2O (1 mL) and transferred on a glass slide.

Drosophila Melanogaster Embryos. *Drosophila Melanogaster* embryos were prepared for the imaging experiments adapting a literature protocol.[82] Specifically, embryos were collected during cellularization, aligned in pairs on glass slides and maintained in a desiccator, together with $CaCl_2$, at ambient temperature for 8 minutes. The slides were covered with a mixture (7:1, v/v) of Series 700 (Sigma H8898) and Series 27 (Sigma H8773) halocarbon oils and transferred individually on the stage of a Leica DMIL LED inverted microscope. A solution of nanoparticles of **13** (5 mg mL^{-1}), containing **3** (50 μg

mL^{-1}), in Dulbecco's PBS (pH = 7.2–7.6) was microinjected in only one embryo of each pair of embryos with a MN151 Narishige micromanipulator. After 1 hour, the slides were mounted on the stage of a Leica SP5 confocal laser-scanning microscope and imaged for 40 minutes.

Acknowledgment. J. G.-A. is grateful for a *Beatriu de Pinós* postdoctoral grant from the *Generalitat de Catalunya* (Spain, 2011 BP-A-00270). F. M. R. acknowledges the National Science Foundation (CAREER Award CHE-0237578, CHE-0749840 and CHE-1049860) for financial support.

Supporting Information Available. Crystallographic data for **1**; emission spectra of **2**, **3**, **5**, **6** and **12**; differential-pulse voltammograms of **1** and **12**; dependence of the emission intensity of **12** on the concentration of **13**; fluorescence images of **3** in PBMA; fluorescence images of nanoparticles of **13**, doped with **3** or **12**, in alginate hydrogels; fluorescence images of nanoparticles of **13**, doped with **3**, in *Drosophila Melanogaster* embryos. This material is available free of charge via the Internet at http://pubs.acs.org.

References

1 (a) Halperin, A.; Tirrell, M.; Lodge, T. P. *Adv. Polym. Sci.* **1992**, *100*, 31–71. (b) Lodge, T. P. *Macromol. Chem. Phys.* **2003**, *204*, 265–273. (c) Moughton, A. O.; Hillmyer, M. A.; Lodge, T. P. *Macromolecules* **2012**, *45*, 2–19.

2 (a) Moffitt, M.; Khougaz, K.; Eisenberg, A. *Acc. Chem. Res.* **1996**, *29*, 95–102. (b) Cameron, N. S.; Corbierre, K. M.; Eisenberg, A. *Can. J. Chem*. **1999**, *77*, 1311–1326.

3 Webber, S. E. *J. Phys. Chem. B* **1998**, *102*, 2618–2626.

4 Riess, G. *Prog. Polym. Sci.* **2003**, *28*, 1107–1170.

5 Okhapkin, I. M.; Makhaeva, E. E.; Khokhlov, A. R. *Adv. Polym. Sci.* **2006**, *195*, 177–210.

6 Kale, T. S.; Klaikherd, A.; Popere, B.; Thayumanavan, S. *Langmuir* **2009**, *25*, 9660−9670.

7 Owen, S. C.; Chan, D. P. Y.; Shoichet, M. S. *Nano Today* **2012**, *7*, 53–65.

8 Bader, H.; Ringsdorf, H.; Schmidt, B. *Angew. Makromol. Chem.* **1984**, *123*, 457–485.

9 Kataoka, K.; Kwon, G. S.; Yokoyama, M.; Okano, T.; Sakurai, Y. *J. Control Release* **1993**, *24*, 119–132.

10 Jones, M.-C.; Leroux, J.-C. *Eur. J. Pharm. Biopharm.* **1999**, *48*, 101–111.

11 Torchilin, V. P. *J. Control Release* **2001**, *73*, 137–172.

12 Adams, M. L.; Lavasanifar, A.; Kwon, G. S. *J. Pharm. Sci.* **2003**, *92*, 1343–1355.

13 Husseini, A. G.; Pitt, W. G. *Adv. Drug Deliv. Rev.* **2008**, *60*, 1137–1152.

14 Mondon, K.; Gurny, R.; Moller, M. *Chimia* **2008**, *62*, 832–840.

15 Park, J. H.; Lee, S.; Kim, J. H.; Park, K.; Kim, K.; Kwon, I. C. *Prog. Polym. Sci.* **2008**, *33*, 113–137.

16 Kim, S.; Shi, Y.; Kim, J. Y.; Park, K.; Cheng, J.-X. *Expert Opin. Drug. Deliv.* **2010**, *7*, 49–62.

17 (a) Chacko, R. T.; Ventura, J.; Zhuang, J.; Thayumanavan, S. *Adv. Drug. Deliv. Rev.* **2012**, *64*, 836–851. (b) Zhuang, J.; Gordon, M. R.; Ventura, J.; Li, L.; Thayumanavan, S. *Chem. Soc. Rev.* **2013**, *42*, 7421–7435.

18 Wang, Y.; Grayson, S. M. *Adv. Drug Deliv. Rev.* **2012**, *64*, 852–865.

19 Lalatsa, A.; Schatzlein, A. G.; Mazza, M.; Thi, B. H. L.; Uchegbu, I. F. *J. Control. Rel.* **2012**, *161*, 523–536.

20 (a) Nicolas, J.; Mura, S.; Brambilla, D.; Mackiewicz, N.; Couvreur, P. *Chem. Soc. Rev.* **2013**, *42*, 1147–1235. (b) Mura, S.; Nicolas, J.; Couvreur, P. *Nat. Mater.* **2013**, *12*, 991–1003.

21 Lu, Y.; Park, K. *Int. J. Pharm.* **2013**, *452*, 198–214.

22 Tyler, J. Y.; Xu, X.-M.; Cheng, J.-X. *Nanoscale* **2013**, *5*, 8821–8836.

23 Wang, D. R.; Wang, X. G. *Prog. Polym. Sci.* **2013**, *38*, 271–301.

24 Gu, L.; Faig, A.; Abdelhamid, D.; Uhrich, K. *Acc. Chem. Res.* **2014**, *47*, 2867–2877.

25 Alakhova, D. Y.; Kabanov, A. V. *Mol. Pharm.* **2014**, *11*, 2566–2578.

26 Makino, A. *Polym. J.* **2014**, *46*, 783–791.

27 Lakowicz, J. R. *Principles of Fluorescence Spectroscopy*; Springer: New York, 2006.

28 Swaminathan, S.; Garcia-Amorós, J.; Fraix, A.; Kandoth, N.; Sortino, S.; Raymo, F. M. *Chem. Soc. Rev.* **2014**, *43*, 4167–4178.

29 Ishikawa-Ankerhold, H. C.; Ankerhold, R.; Drummen, G. P. C. *Molecules* **2012**, *17*, 4047–4132.

30 Mitchison, T. J.; Sawin, K. E.; Theriot, J. A.; Gee, K.; Mallavarapu, A. *Methods Enzymol.* **1998**, *291*, 63–78.

31 Wysocki, L. M.; Lavis, L. D. *Curr. Op. Chem. Biol.* **2011**, *15*, 752–759.

32 Puliti, D.; Warther, D.; Orange, C.; Specht, A.; Goeldner, M. *Bioorg. Med. Chem.* **2011**, *19*, 1023–1029.

33 Li, W.-H.; Zheng, G. *Photochem. Photobiol. Sci.* **2012**, *11*, 460–471.

34 Klán, P.; Šolomek, T.; Bochet, C. G.; Blanc, A.; Givens, R.; Rubina, M.; Popik, V.; Kostikov, A.; Wirz, J. *Chem. Rev.* **2013**, *113*, 119−191.

35 Raymo, F. M. *Phys. Chem. Chem. Phys.* **2013**, *15*, 14840–14850**.**

36 Adams, S. R.; Tsien, R. Y. *Ann. Rev. Phys.* **1993**, *55*, 755–784.

37 Politz, J. C. *Trends Cell Biol.* **1999**, *9*, 284–287.

38 Dirks, R. W.; Molenaar, C.; Tanke, H. J. *Histochem. Cell Biol.* **2001**, *115*, 3–11.

39 Ellis-Davies, G. C. *Nat. Methods* **2007**, *4*, 619–628.

40 Xu, Y.; Melia, T. J.; Toomre, D. T. *Curr. Op. Chem. Biol.* **2011**, *15*, 822–830.

41 Raymo, F. M. *ISRN Phys. Chem.* **2012**, 619251-1–15.

42 Huang, B.; Bates, M.; Zhuang, X. *Ann. Rev. Biochem.* **2009**, *78*, 993–1016.

43 Hell, S. W. *Nat. Methods* **2009**, *6*, 24–32.

44 van de Linde, S.; Heilemann, M.; Sauer, M. *Ann. Rev. Phys. Chem.* **2012**, *63*, 519–540.

45 Ha, T.; Tinnefeld, P. *Ann. Rev. Phys. Chem.* **2012**, *63*, 595–617.

46 Moerner, W. E. *J. Microsc.* **2012**, *246*, 213–220.

47 Raymo, F. M. *J. Phys. Chem. Lett.* **2012**, *3*, 2379–2385.

48 Xu, J.; Chang, J.; Yan, Q.; Dertinger, T.; Bruchez, M. P.; Weiss, S. *J. Phys. Chem. Lett.* **2013**, *4*, 2138−2146.

49 Endesfelder, U.; Heilemann, M. *Nat. Methods* **2014**, *11*, 235–238.

50 (a) Loudet, A.; Burgess, K. *Chem. Rev.* **2007**, *107*, 4891−4932. (b) Kamkaew, A.; Lim, S. H.; Lee, H. B.; Kiew, L. V.; Chung, L. Y.; Burgess, K. *Chem. Soc. Rev.* **2013**, *42*, 77–88.

51 (a) Ziessel, R.; Ulrich, G.; Harriman, A. *New J. Chem*. **2007**, *31*, 496–501. (b) Ulrich, G.; Ziessel, R.; Harriman, A. *Angew. Chem. Int. Ed.* **2008**, *47*, 1184–1201.

52 Benstead, M.; Mehl, G. H.; Boyle, R. W. *Tetrahedron* **2011**, *67*, 3573–3601.

53 Boens, N.; Leen, V.; Dehaen, W. *Chem. Soc. Rev.* **2012**, *41*, 1130–1172.

54 Lu, H.; Mack, J.; Yang, Y.; Shen, Z. *Chem. Soc. Rev.* **2014**, *43*, 4778–4823.

55 Ni, Y.; Wu, J. *Org. Biomol. Chem.* **2014**, *12*, 3774–3791.

56 Kobayashi, T.; Komatsu, T.; Kamiya, M.; Campos, C.; González-Gaitán, M.; Terai, T.; Hanaoka, K.; Nagano, T.; Urano, Y. *J. Am. Chem. Soc.* **2012**, *134*, 11153−11160.

57 (a) Shaban Ragab, S.; Swaminathan, S.; Deniz, E.; Captain, B.; Raymo, F. M. *Org. Lett.* **2013**, *15*, 3153–3157. (b) Shaban Ragab, S.; Swaminathan, S.; Baker, J. D.; Raymo, F. M. *Phys. Chem. Chem. Phys*. **2013**, *15*, 14851–14855.

58 Huang, B.; Bates, M.; Zhuang, X. *Ann. Rev. Biochem.* **2009**, *78*, 993–1016.

59 Hell, S. W. *Nat. Methods* **2009**, *6*, 24–32.

60 van de Linde, S.; Heilemann, M.; Sauer, M. *Ann. Rev. Phys. Chem.* **2012**, *63*, 519–540.

61 Ha, T.; Tinnefeld, P. *Ann. Rev. Phys. Chem.* **2012**, *63*, 595–617.

62 Moerner, W. E. *J. Microsc.* **2012**, *246*, 213–220.

63 Raymo, F. M. *J. Phys. Chem. Lett.* **2012**, *3*, 2379–2385.

64 Xu, J.; Chang, J.; Yan, Q.; Dertinger, T.; Bruchez, M. P.; Weiss, S. *J. Phys. Chem. Lett.* **2013**, *4*, 2138−2146.

65 (a) Deniz, E.; Sortino, S.; Raymo, F. M. *J. Phys. Chem. Lett.* **2010**, *1*, 3506–3509. (b) Deniz, E.; Tomasulo, M.; Cusido, J.; Sortino, S.; Raymo, F. M. *Langmuir* **2011**, *27*, 11773–11783. (c) Deniz, E.; Cusido, J.; Swaminathan, S.; Battal, M.; Impellizzeri, S.; Sortino, S.; Raymo, F. M. *J. Photochem. Photobiol. A* **2012**, 229, 20–28. (d) Deniz, E.; Tomasulo, M.; Cusido, J.; Yildiz, I.; Petriella, M.; Bossi, M. L.; Sortino, S.; Raymo, F. M.; *J. Phys. Chem. C* **2012**, *116*, 6058−6068.

(e) Deniz, E.; Battal, M.; Cusido, J.; Sortino, S.; Raymo, F. M. *Phys. Chem. Chem. Phys.* **2012**, *14*, 10300–10307. (f) Cusido, J.; Battal, M.; Deniz, E.; Yildiz, I.; Sortino, S.; Raymo, F. M. *Chem. Eur. J.* **2012**, *18*, 10399–10407. (g) Swaminathan, S.; Petriella, M.; Deniz, E.; Cusido, J.; Baker, J. D.; Bossi, M. L.; Raymo, F. M. *J. Phys. Chem. A* **2012**, *116*, 9928–9933. (h) Deniz, E.; Kandoth, N.; Fraix, A.; Cardile, V.; Graziano, A. C. E.; Lo Furno, D.; Gref, R.; Raymo, F. M.; Sortino, S.; *Chem. Eur. J.* **2012**, *18*, 15782–15787. (i) Raymo, F. M. *Isr. J. Chem.* **2013**, *53*, 247–255. (j) Petriella, M.; Deniz, E.; Swaminathan, S.; Roberti, M. J.; Raymo, F. M.; Bossi, M. L. *Photochem. Photobiol.* **2013**, *89*, 1391–1398. (k) Garcia-Amorós, J.; Swaminathan, S.; Raymo, F. M. *Dyes Pigments* **2014**, *106*, 71–73. (l) Garcia-Amorós, J.; Swaminathan, S.; Sortino, S.; Raymo, F. M. *Chem. Eur. J.* **2014**, *20*, 10276–10284.

66 (a) Tomasulo, M.; Sortino, S.; Raymo, F. M. *Org. Lett.* **2005**, *7*, 1109–1112. (b) Tomasulo, M.; Sortino, S.; White, A. J. P.; Raymo, F. M. *J. Org. Chem.* **2005**, *70*, 8180–8189. (c) Raymo, F. M. *J. Phys. Chem. A* **2012**, *116*, 11888–11895.

67 Goeldner, M.; Givens, R. (Eds.) *Dynamic Studies in Biology: Phototriggers, Photoswitches and Caged Biomolecules*; Wiley–VCH: Weinheim, 2005.

68 The free-energy change ($\Delta G°$) for the two electron transfer processes was calculated with equation (1) (Kavarnos, G. J. *Fundamentals of Photoinduced Electron Transfer*; VCH: New York, 1993). The oxidation potential (E_{Ox}) of the donor and the reduction potential (E_{Red}) of the acceptor in both instances were determined from the differential pulse voltammograms (Figure S2) of **1** and **12**. The energy change (ΔE_{00}) for the $S_0 \rightarrow S_1$ transition of the BODIPY chromophore was estimated to be +2.35 eV from the absorption and emission spectra of **12**. The donor–acceptor distance (d) was approximated to 0.5 nm in both instances.

$$\Delta G° = e\,E_{Ox} - e\,E_{Red} - \Delta E_{00} - \frac{e^2}{4\,\pi\,\varepsilon_0\,\varepsilon_r\,d} \qquad (1)$$

69 Macromolecule **13** was synthesized from the corresponding methacrylate monomers (ref. 71a), adapting a literature protocol (ref. 78) for atom-transfer radical polymerization. Gel permeation chromatography (GPC) and ^{1}H NMR spectroscopy were employed to determine M_n and the ratio between the hydrophobic and hydrophilic chains respectively.

70 The critical concentration of **13**, required to encourage the assembly of nanoparticles, was estimated from the dependence of the emission intensity of **12** on the polymer concentration (Figure S3), adapting a literature protocol (ref. 71b). Dynamic light scattering (DLS) measurements were employed to determine the average hydrodynamic diameter of the nanoparticles.

71 (a) Yildiz, I.; Impellizzeri, S.; Deniz, E.; McCaughan, B.; Callan, J. F.; Raymo, F. M. *J. Am. Chem. Soc.* **2011**, *133*, 871–879. (b) Swaminathan, S.; Fowley, C.; McCaughan, B.; Cusido, J.; Callan, J. F.; Raymo, F. M. *J. Am. Chem. Soc.* **2014**, *136*, 7907–7913.

72 Solutes of various dimensions and shapes, including relatively large biomolecules, are known to diffuse through alginate hydrogels (ref. 73–75). These materials hold large amounts of water within intricate networks of polyanionic alginate chains bridged by divalent calcium cations.

73 (a) Quignard, F.; Valentinw, R.; Di Renzo, F. *New J. Chem.* **2008**, *32*, 1300–1310. (b) Quignard, F.; Di Renzo, F.; Guibal, E. *Top. Curr. Chem.* **2010**, *294*, 165–197. (c) Robitzer, M.; Quignard, F. *Chimia* **2011**, *65*, 81–84.

74 Oh, J. K.; Lee, D. I.; Park, J. M. *Prog. Polym. Sci.* **2009**, *34*, 1261–1282.

75 García-González, C. A.; Alnaief, M.; Smirnova, I. *Carbohydr. Polym.* **2011**, *86*, 1425–1438.

76 In principle, the photoactivatable guests can leak out of their supramolecular hosts (Jiwpanich, S.; Ryu, J.-H.; Bickerton, S.; Thayumanavan, S. *J. Am. Chem. Soc.* **2010**, *132*, 10683–10685) and diffuse across the sample. The hydrophobic character of **3** and **6**, however, translates into aqueous solubilities in the subpicomolar regime. At such low concentration levels, the fluorescence of any

activated guest, which might be present outside the nanocarriers, is undetectable under the experimental conditions employed to acquire the images in Figure 11. As a result, the observed intense emission can only be associated with the large fraction of fluorophores encapsulated within the supramolecular containers.

77 Campos-Ortega, J. A.; Hartenstein, V. *The Embryonic Development of Drosophila Melanogaster*; Springer: Berlin, 1997.

78 Zhu, G.; Zhang, L.; Zhang, Z.; Zhu, J.; Tu, Y.; Cheng, Z.; Zhu, X. *Macromolecules* **2011**, *44*, 3233–3239.

79 Scaiano, J. C. *Handbook of Organic Photochemistry*; CRC Press: Florida, 1989.

80 Apex2 Version 2.2-0 and SAINT+ Version 7.46A; Bruker Analytical X-ray System, Inc., Madison, Wisconsin, USA, 2007.

81 (a) Sheldrick, G. M. SHELXTL Version 6.1; Bruker Analytical X-ray Systems, Inc., Madison, Wisconsin, USA, 2000. (b) Sheldrick, G. M. *Acta Cryst*. **2008**, *A64*, 112–122.

82 Spradling, A. C.; Rubin, G. M. *Science* **1982**, *218*, 341–347.

Table 1. Photochemical and photophysical parameters of **1**–**3**, **5**, **6** and **12** in MeCN at 25 °C.

	λ_{Ab} [a] (nm)	ε [b] ($mM^{-1}\ cm^{-1}$)	λ_{Em} [a] (nm)	ϕ_F [c]	$\varepsilon \times \phi_F$ [d] ($mM^{-1}\ cm^{-1}$)	ϕ_A [c]
1	333	2	—	—	—	0.043
2	520	84	555	0.06	5	0.002
3	548	111	562	0.07	8	0.002
5	534	88	620	<0.01	<1	—
6	588	134	602	0.50	67	—
12	521	86	534	0.77	66	—

[a] Wavelengths at the absorption (λ_{Ab}) and emission (λ_{Em}) maxima. [b] Molar absorption coefficient at λ_{Ab}. [c] Fluorescence (ϕ_F) and activation (ϕ_A) quantum yields. [d] Brightness at λ_{Ab}.

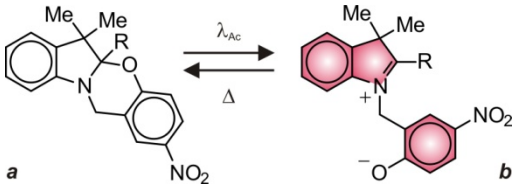

Figure 1. Reversible opening of an oxazine ring (***a***) to form a zwitterionic isomer (***b***) under illumination at an activating wavelength (λ_{Ac})**.**

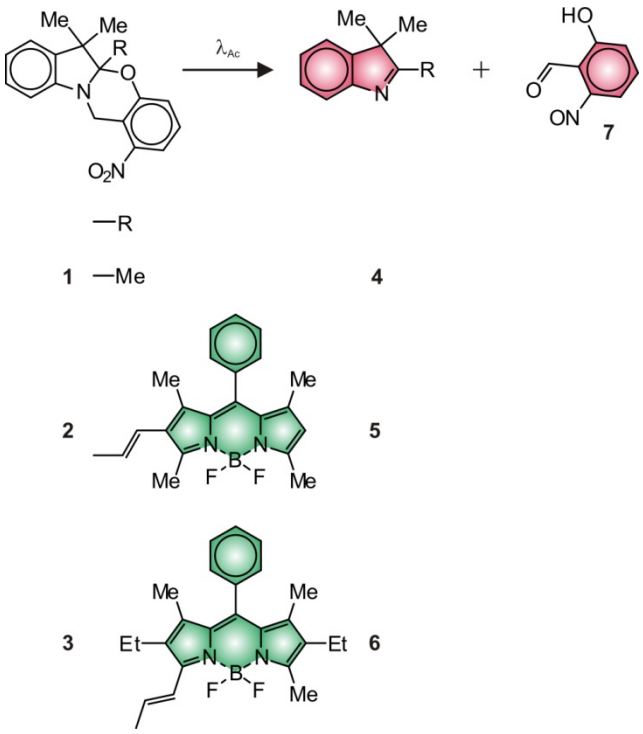

Figure 2. Irreversible opening of the oxazine ring of **1**–**3** to form **4**–**6** and **7** under illumination at an activating wavelength (λ_{Ac}).

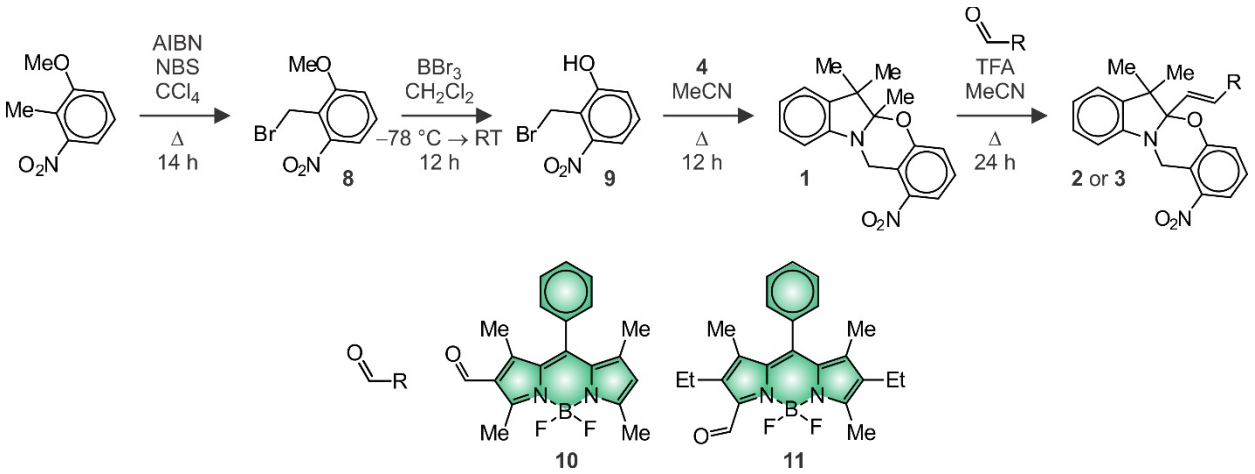

Figure 3. Synthesis of **1**–**3**.

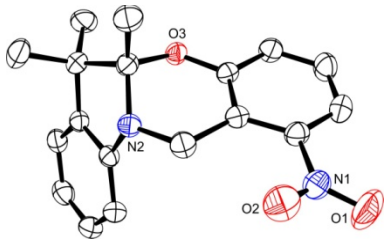

Figure 4. ORTEP representation of the geometry adopted by **1** in single crystals, showing 40% thermal ellipsoid probability.

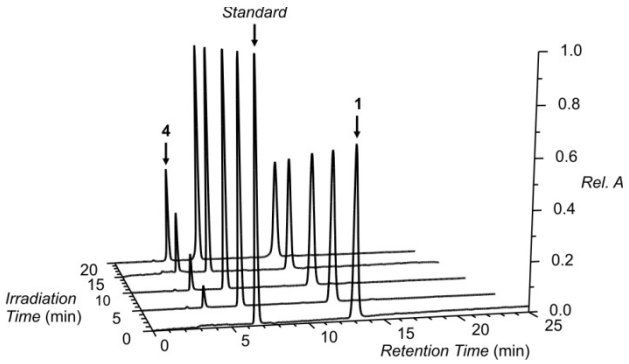

Figure 5. HPLC traces [1.0 mL min^{-1}, BDS, MeCN/H_2O (60:40, v/v), 250 nm] recorded before and during the photolysis (350 nm, 4.88 mW cm^{-2}) of a solution of **1** (0.1 mM, MeCN, 25 °C).

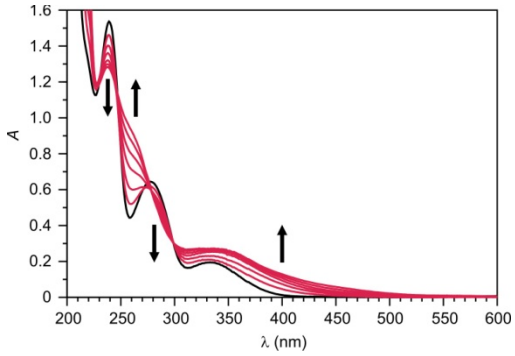

Figure 6. Absorption spectra recorded before and during the photolysis (350 nm, 4.88 mW cm^{-2}) of a solution (0.1 mM, MeCN, 25 °C) of **1** for 30 min.

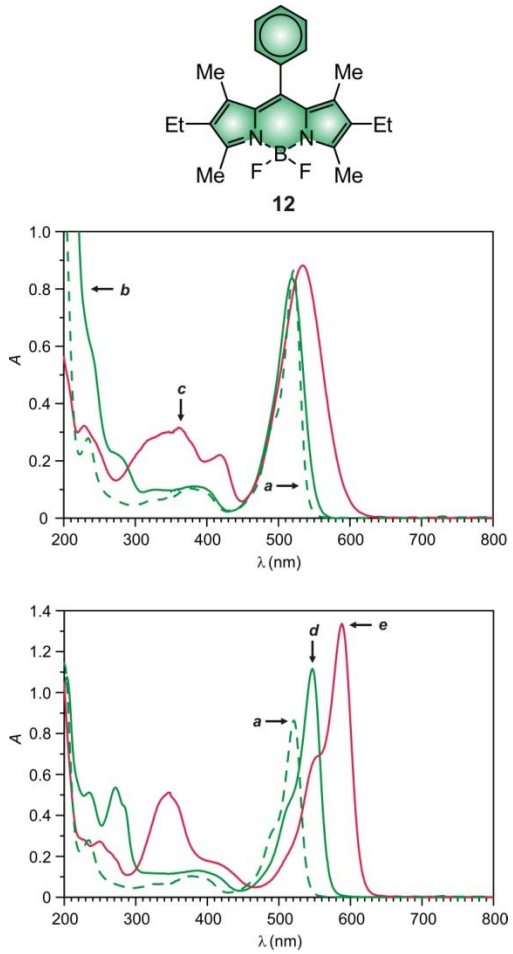

Figure 7. Absorption spectra (10 μM, MeCN, 25 °C) of **12** (***a***), **2** (***b***), **5** (***c***), **3** (***d***) and **6** (***e***).

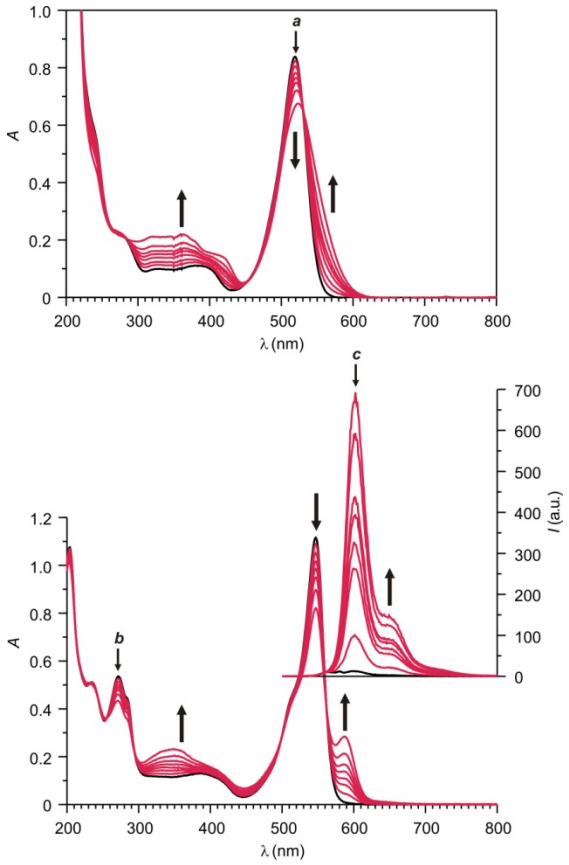

Figure 8. Absorption spectra recorded before and during the photolysis (350 nm, 4.88 mW cm^{-2}) of solutions (0.1 mM, MeCN, 25 °C) of **2** (***a***) and **3** (***b***) for 10 min. Corresponding emission spectra (***c***, λ_{Ex} = 580 nm) in the case of **3**.

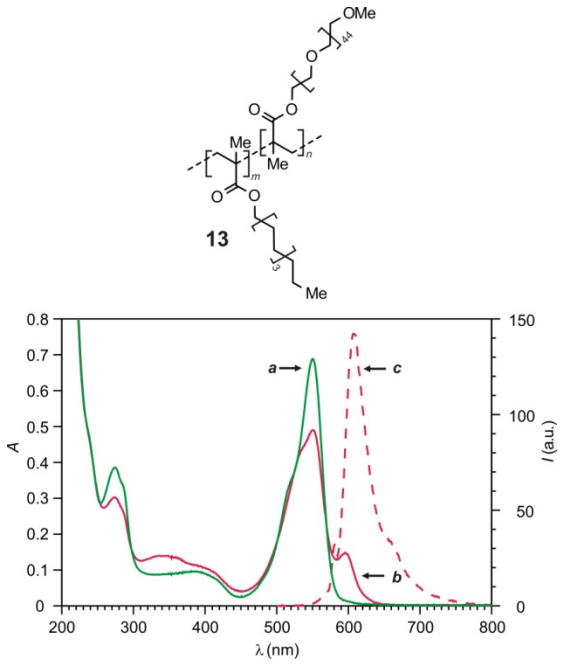

Figure 9. Absorption spectra of nanoparticles of **13** (630 μg mL^{-1}), doped with **3** (5 μg mL^{-1}), recorded before (***a***) and after (***b***) photolysis (350 nm, 4.88 mW cm^{-2}) for 10 min in PBS (pH = 7.4) at 25 ºC and the corresponding emission spectrum (***c***, λ_{Ex} = 580 nm) after irradiation.

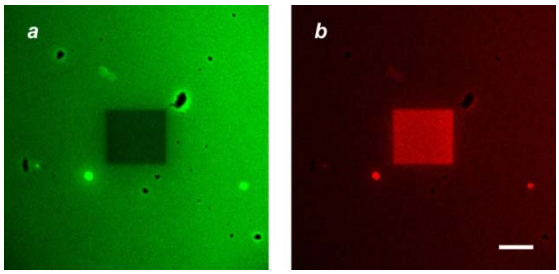

Figure 10. Fluorescence images (scale bar = 100 μm) of a PBMA film, doped with **3** (0.25% w/w), recorded with either a λ_{Ex} of 514 nm and a detection window of 530–650 nm (***a***) or a λ_{Ex} of 594 nm and a detection window of 610–700 nm (***b***) after activation of a rectangular region at a λ_{Ac} of 405 nm.

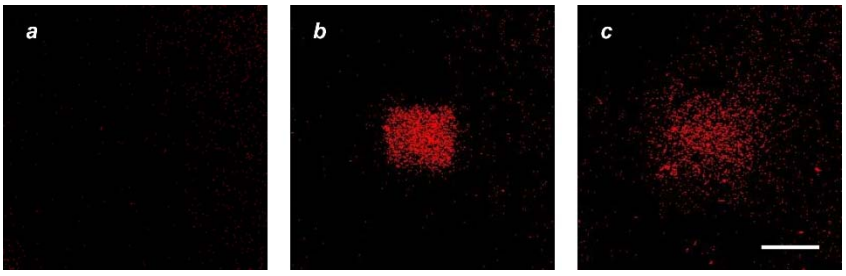

Figure 11. Fluorescence images (scale bar = 50 μm) of an alginate hydrogel, doped with nanoparticles of **13** (250 μg mL^{-1}) containing **3** (2.5 μg mL^{-1}), recorded with a λ_{Ex} of 594 nm and a detection window of 610–700 nm before (***a***) and after (***b***) activation of a rectangular region at a λ_{Ac} of 405 nm for 10 s and 630 s after activation (***c***).

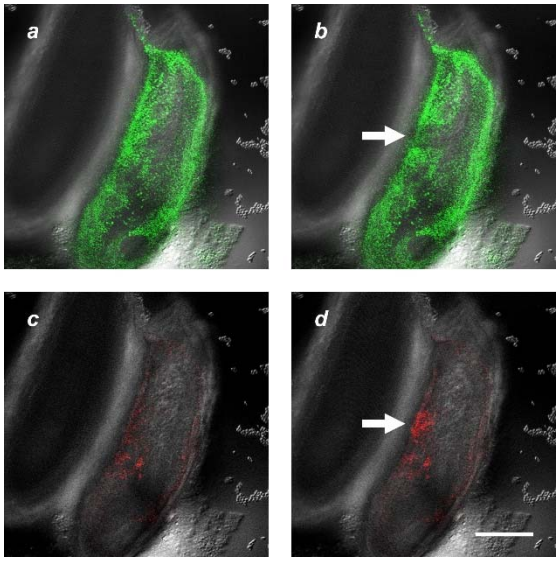

Figure 12. Overlaid fluorescence and transmittance images (scale bar = 100 μm) of two adjacent *Drosophila Melanogaster* embryos, one of which was microinjected with a solution of nanoparticles of **13** (5 mg mL^{-1}) containing **3** (50 μg mL^{-1}) in Dulbecco's PBS, recorded with either a λ_{Ex} of 514 nm and a detection window of 530–650 nm (***a*** and ***b***) or a λ_{Ex} of 594 nm and a detection window of 610–700 nm (***c*** and ***d***) before (***a*** and ***c***) and after (***b*** and ***d***) activation of the indicated area at a λ_{Ac} of 405 nm for 10 s.

40

Graphical Abstract